

Characterization of Blue-Green Light Non-Line-of-Sight Transmission in Seawater

Xizheng Ke^{1,2,3}, Gang Li^{1*}

¹Faculty of Automation and Information Engineering, Xi'an University of Technology, Xi'an, China

²Shaanxi Civil-Military Integration Key Laboratory of Intelligence Collaborative Networks, Xi'an, China

³College of Physics and Electronics, Shaanxi University of Technology, Hanzhong, China

Email: *2289125469@qq.com

How to cite this paper: Ke, X.Z. and Li, G. (2022) Characterization of Blue-Green Light Non-Line-of-Sight Transmission in Seawater. *Optics and Photonics Journal*, 12, 234-252. <https://doi.org/10.4236/opj.2022.1211018>

Received: October 28, 2022

Accepted: November 20, 2022

Published: November 23, 2022

Copyright © 2022 by author(s) and Scientific Research Publishing Inc.

This work is licensed under the Creative Commons Attribution International License (CC BY 4.0).

<http://creativecommons.org/licenses/by/4.0/>



Open Access

Abstract

The blue-green light in the 450 nm to 550 nm band is usually used in underwater wireless optical communication (UWOC). The blue-green light transmission in seawater is scattered by the seawater effect and can achieve communication in non-line-of-sight (NLOS) transmission mode. Compared to line-of-sight (LOS) transmission, NLOS transmission does not require alignment and can be adapted to various underwater environments. The scattering coefficients of seawater at different depths are different, which makes the scattering of light in different depths of seawater different. In this paper, the received optical power and bit error rate (BER) of the photodetector (PD) were calculated when the scattering coefficients of blue-green light in seawater vary from large to small with increasing depth for NLOS transmission. The results show that blue-green light in different depths of seawater in the same way NLOS communication at the same distance, the received optical power and BER at the receiver are different, and the received optical power of green light is greater than that of blue light. Increasing the forward scattering coverage of the laser will suppress the received optical power of the PD, so when performing NLOS communication, appropriate trade-offs should be made between the forward scattering coverage of the laser and the received optical power.

Keywords

Underwater Wireless Optical Communication, Non-Line-of-Sight Transmission, Scattering Coefficient, Received Optical Power, Bit Error Rate

1. Introduction

Underwater communication (UC) methods include underwater acoustic com-

munication (UAC) and underwater radio frequency (RF) communication. UAC has a low transmission rate, high latency, and cannot achieve real-time communication. Underwater RF communication uses electromagnetic waves in the frequency range of 30 Hz to 300 Hz, but the modulation bandwidth is very narrow, which severely limits the communication rate. Optical communications (OC) is a new type of UC that is of interest because of its fast transmission rate and large channel capacity. Since Duntley's discovery in 1963 of the existence of a transmission window for blue-green light in the 450 nm to 550 nm wavelength band in seawater [1], more and more researchers have been studying underwater wireless optical communication (UWOC).

Light transmission in seawater is attenuated by seawater absorption and scattering. The absorption and scattering of light by seawater are related to the wavelength of light and the type of water quality [2] [3] [4] [5], whereby researchers usually gave typical values of absorption coefficients and scattering coefficients of seawater depending on the type of water quality [5] [6] [7]. However, as the research progressed, researchers found that the scattering of light by seawater is also related to the temperature [8], salinity [9], pressure [10], and the type and concentration of suspended particles contained in the seawater [11]. In UWOC, when the line-of-sight (LOS) communication link of laser and photo-detector (PD) is obstructed by obstacles, the communication can be realized by non-line-of-sight (NLOS) transmission method. The NLOS transmission reduces the transmitter pointing and receiver tracking requirements and enriches the working scenario of UWOC. NLOS UWOC was first proposed by Arnon *et al.* in 2009 [12]. Arnon *et al.* pointed out that point-to-multipoint NLOS UWOC can be achieved through back-reflection at the ocean-air interface [12]. In 2014, Jagadeesh *et al.* investigated the channel impulse response (CIR) of NLOS UWOC system using Monte Carlo (MC) method and Henyey-Greenstein (HG) phase function considering different water quality types and detector reception field of view [13]. In 2015, Liu *et al.* used the MC method to study the CIR and link loss of NLOS UWOC systems in coastal and harbor waters considering the elevation angles of the transmitter and receiver as well as the optical wavelength [14]. In 2019, Sait *et al.* studied the effect of turbulence and different bubble populations generated by temperature gradient changes on NLOS UWOC channels [15]. In 2020, Priyalakshmi *et al.* proposed channel estimation and error correction techniques for vertical NLOS UWOC system based on multiple-in multiple-out orthogonal frequency division multiplexing (MIMO-OFDM) and compared the channel capacity, bit error rate (BER), signal-to-noise ratio (SNR), data rate, received power and mean-square error (MSE) of the system under four water quality types [16]. In 2021, Sait *et al.* found that salt particles in seawater cause light scattering and increasing salt concentration can increase the distance of NLOS communication, so Sait *et al.* investigated the effect of vertical salinity gradient on NLOS UWOC and modeled the NLOS channel [17].

The absorption coefficients and scattering coefficients of seawater in the above-mentioned scholars' studies use typical values under different water qual-

ity types, without considering the differences in scattering coefficients of seawater at different pressures (*i.e.*, different depths). And many current UWOC studies are also based on typical values of seawater absorption and scattering coefficients for different water quality types. Accordingly, this paper analyzes the received optical power and BER of the PD when the blue-green light NLOS transmission at different depths by establishing a single scattering link model, which provides a theoretical basis for setting the parameters of transmitting optical power, transmit deflection angle of the laser and receive deflection angle of the PD according to the seawater environment in NLOS UWOC.

The remainder of the paper is organized as follows. In Section II, we calculated the absorption and scattering coefficients of seawater at different depths, and the scattering angle of scattered photons from seawater. In Section III, we calculate the forward scattering coverage, received optical power and BER of the PD for blue-green light in class a form and class b form for NLOS transmission in seawater. In Section IV, set simulation parameters and perform simulation analysis on the calculation results. Finally, Section V concludes the paper.

2. Absorption and Scattering of Seawater

2.1. Absorption of Seawater

The absorption of seawater mainly includes the absorption of pure seawater, chlorophyll and yellow matter, expressed by the absorption coefficient $a_{sea}(\lambda)$; the scattering of seawater mainly includes the scattering of pure seawater, chlorophyll, small particles and large particles, expressed by the scattering coefficient $b_{sea}(\lambda)$. Where the scattering of seawater is divided into forward scattering and backscattering, which are expressed by the forward scattering coefficient $b_{sea}(\lambda)$ and the backscattering coefficient $b_{seab}(\lambda)$, respectively.

The absorption of pure seawater includes the absorption of pure water and salt in seawater. Assuming that the absorption of salt is negligible in the visible wavelength band [6], the absorption coefficient of pure seawater for light in the visible wavelength band is approximately equal to the absorption coefficient of pure water. In 1997, Pope *et al.* gave the absorption coefficients of pure water for light in the 380 nm to 727.5 nm band, where the absorption coefficients of pure water are 0.00922 m^{-1} for blue light at 450 nm and 0.0409 m^{-1} for green light at 520 nm [3].

The absorption coefficient of chlorophyll $a_c(\lambda)$ is [11]

$$a_c(\lambda) = a_c^0(\lambda) \left(\frac{C_c}{C_c^0} \right)^{0.602} \quad (1)$$

where $a_c^0(\lambda)$ is the specific absorption coefficient of chlorophyll, C_c is the concentration of chlorophyll, $C_c^0 = 1 \text{ mg/m}^3$. Reference [18] gave the values of $a_c^0(\lambda)$ at different light wavelengths, $a_c^0(450) = 0.944 \text{ m}^{-1}$ and $a_c^0(520) = 0.528 \text{ m}^{-1}$.

Yellow matter is a kind of humus produced by the decay of animals and

plants, and is a kind of chromophoric dissolvable organic matter (CDOM) with complex structure dissolved in seawater. The absorption coefficient of the yellow substance $a_y(\lambda)$ is [11]

$$a_y(\lambda) = a_f^0 C_f \exp(-k_f \lambda) + a_h^0 C_h \exp(-k_h \lambda) \quad (2)$$

where the specific absorption coefficient of fulvic acid $a_f^0 = 35.959 \text{ m}^2/\text{mg}$, the specific absorption coefficient of humic acid $a_h^0 = 18.828 \text{ m}^2/\text{mg}$, $k_f = 0.0189 \text{ nm}^{-1}$, $k_h = 0.01105 \text{ nm}^{-1}$, C_f is the concentration of fulvic, and C_h is the concentration of humic. Haltrin pointed out that C_f and C_h are related to C_c , and can be expressed by C_c [11]. Therefore, the absorption coefficient of seawater $a_{sea}(\lambda)$ is

$$a_{sea}(\lambda) = a_{ps}(\lambda) + a_c(\lambda) + a_y(\lambda) \quad (3)$$

where $a_{ps}(\lambda)$ is the absorption coefficient of pure water.

2.2. Scattering of Seawater

The scattering coefficient of pure seawater $b_{ps}(\lambda)$ is [10]

$$b_{ps}(\lambda) = \frac{8\pi}{3} \frac{2 + \delta}{1 + \delta} \beta(90^\circ) \quad (4)$$

where $\delta = 0.039$ is the depolarization rate of pure seawater [9], and the expression of $\beta(90^\circ)$ is [8]

$$\beta(90^\circ) = \frac{\pi^2 k_B T}{2\lambda^4} \frac{6 + 6\delta}{6 - 7\delta} \left[\frac{-g_{pp}}{g_p} h_a^2(n) + \frac{g_p}{g_{SS}} h_c^2(n) \right] \quad (5)$$

where k_B is the Boltzmann constant, T is the absolute temperature of seawater, λ is the wavelength of light, g_p and g_{pp} are the first and second order partial derivatives of the Gibbs energy of seawater $g(S_A, T_c, p)$ with respect to the pressure p , g_{SS} is the second order partial derivative of $g(S_A, T_c, p)$ with respect to the absolute salinity S_A , T_c is the temperature of seawater, and n is the refractive index of seawater. n is related to λ , T_c , S (the salinity of seawater) and p . Reference [8] gave the expression of $g(S_A, T_c, p)$, therefore

$$g_p = \frac{\partial g(S_A, T_c, p)}{\partial p} = \sum_{j=0}^7 \sum_{k=0}^6 \frac{k g_{0jk}^w}{p_u^k} \left(\frac{T_c}{T_u} \right)^j p^{k-1} + \sum_{j=0}^6 \sum_{k=0}^5 \left[g_{1jk}^s \left(\frac{S_A}{S_u} \right) \ln \left(\frac{S_A}{S_u} \right)^{0.5} + \sum_{i=2}^7 g_{ijk}^s \left(\frac{S_A}{S_u} \right)^{0.5i} \right] \frac{k}{p_u^k} \left(\frac{T_c}{T_u} \right)^j p^{k-1} \quad (6)$$

$$g_{pp} = \frac{\partial^2 g(S_A, T_c, p)}{\partial p^2} = \sum_{j=0}^7 \sum_{k=0}^6 \frac{k(k-1) g_{0jk}^w}{p_u^k} \left(\frac{T_c}{T_u} \right)^j p^{k-2} + \sum_{j=0}^6 \sum_{k=0}^5 \left[g_{1jk}^s \left(\frac{S_A}{S_u} \right) \ln \left(\frac{S_A}{S_u} \right)^{0.5} + \sum_{i=2}^7 g_{ijk}^s \left(\frac{S_A}{S_u} \right)^{0.5i} \right] \frac{k(k-1)}{p_u^k} \left(\frac{T_c}{T_u} \right)^j p^{k-2} \quad (7)$$

$$g_{ss} = \frac{\partial^2 g(S_A, T_c, p)}{\partial S_A^2} = \sum_{j=0}^6 \sum_{k=0}^5 \left[\frac{0.5}{S_u S_A} g_{1jk}^s + \sum_{i=2}^7 \frac{0.5i(0.5i-1)}{S_u^{0.5i}} g_{ijk}^s S_A^{(0.5i-2)} \right] \left(\frac{T_c}{T_u} \right)^j \left(\frac{p}{p_u} \right)^k \quad (8)$$

where $T_u = 40^\circ\text{C}$, $p_u = 10^8\text{ Pa}$, $S_u = 40.188617\text{ g/kg}$. References [19] [20] gave the values of the coefficients g_{0jk}^w and g_{ijk}^s , respectively. The expressions of $h_d(n)$ and $h_c(n)$ are [8]

$$h_d(n) = (n^2 - 1) \left[1 + \frac{2}{3}(n^2 + 2) \left(\frac{n^2 - 1}{3n} \right)^2 \right] \quad (9)$$

$$h_c(n) = 2n \frac{\partial n}{\partial S_A} \quad (10)$$

Reference [8] gave the expression of n . The forward scattering coefficient and backscattering coefficient of pure seawater are equal, *i.e.*, $b_{psf}(\lambda) = b_{psb}(\lambda) = 0.5b_{ps}(\lambda)$ [10]. The pressure p of seawater is related to the depth d as [21]

$$d = \frac{g(S_A, T_c, p) - g(S_A, T_c, 0)}{g_s + 0.5\gamma p} \quad (11)$$

where $\gamma = 2.226 \times 10^{-6}\text{ ms}^{-2}/\text{db}$, g_s is the first order partial derivative of the seawater Gibbs energy $g(S_A, T_c, p)$ with respect to the absolute salinity S_A .

$$g_s = \frac{\partial g(S_A, T_c, p)}{\partial S_A} = \sum_{j=0}^6 \sum_{k=0}^5 \left\{ \frac{g_{1jk}^s}{S_u} \ln \left(\frac{S_A}{S_u} \right)^{0.5} + 0.5 \frac{g_{1jk}^s}{S_u} + \sum_{i=2}^7 0.5i \frac{g_{ijk}^s}{S_u} \left(\frac{S_A}{S_u} \right)^{0.5i-1} \right\} \times \left(\frac{T_c}{T_u} \right)^j \left(\frac{p}{p_u} \right)^k \quad (12)$$

The scattering coefficient of chlorophyll $b_c(\lambda)$ is [11]

$$b_c(\lambda) = 0.3 \left(\frac{550}{\lambda} \right) C_c^{0.62} \quad (13)$$

Reference [22] gave the probability of backscattering by chlorophyll b_{pc} . b_{pc} multiplied by $b_c(\lambda)$ is the backscattering coefficient of chlorophyll $b_{cb}(\lambda)$. $b_c(\lambda)$ minus $b_{cb}(\lambda)$ is the forward scattering coefficient of chlorophyll $b_{cf}(\lambda)$.

The scattering coefficients of small particles $b_s(\lambda)$ with density 2 g/m^3 and large particles $b_l(\lambda)$ with 1 g/m^3 are [11] [23]

$$b_s(\lambda) = b_s^0(\lambda) C_s \quad (14)$$

$$b_l(\lambda) = b_l^0(\lambda) C_l \quad (15)$$

$b_s^0(\lambda)$ and $b_l^0(\lambda)$ are the spectral dependencies for scattering coefficients of small particles and large particles, respectively. And their values were given in reference [11]. C_s and C_l are the concentrations of small and large particles, and they can be expressed by C_c [11]. The probability of backscattering by small particles $B_s = 0.039$ and large particles $B_l = 6.4 \times 10^{-4}$ [11]. Therefore, the backscat-

tering coefficients of small particles $b_{sb}(\lambda)$ and large particles $b_{lb}(\lambda)$ can be obtained by multiplying B_s by $b_s(\lambda)$ and B_l by $b_l(\lambda)$, respectively. $b_s(\lambda)$ minus $b_{sb}(\lambda)$ and $b_l(\lambda)$ minus $b_{lb}(\lambda)$ are the forward scattering coefficients of small particles $b_{sf}(\lambda)$ and large particles $b_{lf}(\lambda)$, respectively.

The forward scattering coefficient $b_{seaf}(\lambda)$ and backscattering coefficient $b_{seab}(\lambda)$ of seawater are

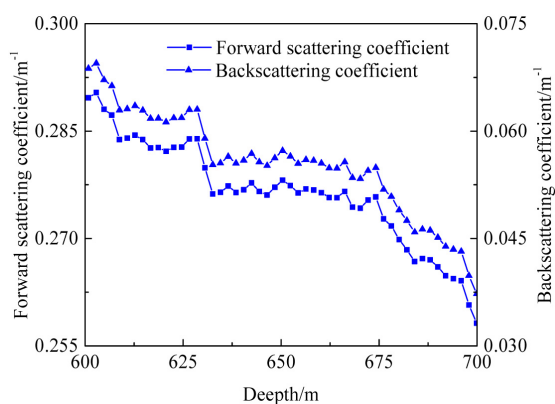
$$b_{seaf}(\lambda) = b_{psf}(\lambda) + b_{cf}(\lambda) + b_{sf}(\lambda) + b_{lf}(\lambda) \quad (16)$$

$$b_{seab}(\lambda) = b_{psb}(\lambda) + b_{cb}(\lambda) + b_{sb}(\lambda) + b_{lb}(\lambda) \quad (17)$$

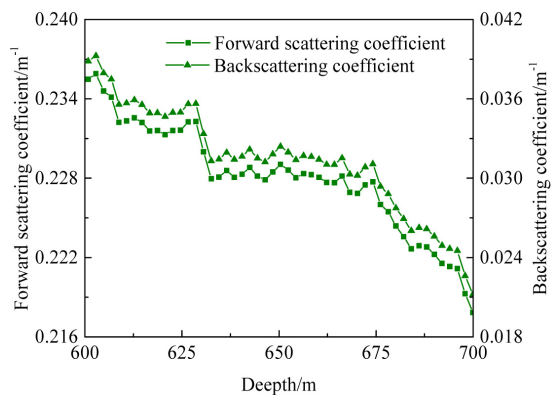
$a_{sea}(\lambda)$ plus $b_{sea}(\lambda)$ is the extinction coefficient of seawater $c_{sea}(\lambda)$.

$$c_{sea}(\lambda) = a_{sea}(\lambda) + b_{sea}(\lambda) = a_{sea}(\lambda) + b_{seaf}(\lambda) + b_{seab}(\lambda) \quad (18)$$

Copernicus Marine Service provides the pressure, temperature and salinity values of seawater in most of the global sea area. In this paper, the characteristics of blue-green light during NLOS transmission at different depths in the 24.5°N, 23.8°W sea area are analyzed as an example. Assuming the chlorophyll concentration $C_c = 0.25 \text{ mg/m}^3$, **Figure 1** shows the forward scattering coefficients and backscattering coefficients of 450 nm blue light and 520 nm green light by seawater in the depth range of 600 m to 700 m at 24.5°N, 23.8°W sea area.



(a)



(b)

Figure 1. Forward scattering coefficients and backscattering coefficients of seawater for 450 nm blue light and 520 nm green light. (a) $\lambda = 450 \text{ nm}$; (b) $\lambda = 520 \text{ nm}$.

Figure 1 shows the forward scattering coefficients and backscattering coefficients of seawater on blue-green light are in an overall decreasing trend with increasing depth, indicating that the scattering effect of seawater on blue-green light is decreasing with increasing depth. The forward scattering coefficients of seawater for blue-green light at the same depth is greater than the backscattering coefficients, indicating that the scattering of seawater for blue-green light tends to be forward scattering.

An important aspect of the transmission of blue-green light in seawater is the determination of the scattering angle of the scattered photons from seawater. In this paper, the scattering angle of the scattered photons from seawater is calculated using the HG phase function [24] [25].

$$\begin{aligned}\chi_\beta &= \int_0^{\theta_s} P_{HG}(\theta, g) \sin \theta d\theta \\ &= \int_0^{\theta_s} \frac{1-g^2}{4\pi(1+g^2-2g\cos\theta)^{\frac{3}{2}}} \sin \theta d\theta\end{aligned}\quad (19)$$

where the upper limit of integration θ_s is the scattering angle to be sought, θ is the scattering angle of the scattered photons from seawater, $P_{HG}(\theta, g)$ is the HG phase function, χ_β is a random number uniformly distributed on $[0, \pi]$, and g is an asymmetry factor. g is related to the backscattering ratio b_p of the seawater [25].

$$b_p = \frac{1-g}{2g} \left(\frac{1+g}{\sqrt{1+g^2}} - 1 \right) \quad (20)$$

The backscattering ratio is defined as the ratio of the backscattering coefficient to the scattering coefficient.

$$b_p = \frac{b_{seab}(\lambda)}{b_{sea}(\lambda)} \quad (21)$$

Bringing Equations (20) and (21) into Equation (19) yields

$$\cos \theta_s = \frac{1+g^2 - \left[\frac{1-g^2}{1+g-4\pi g \chi_\beta} \right]^2}{2g} \quad (22)$$

The backscattering coefficients and scattering coefficients of seawater at different depths are different, so the backscattering ratio b_p and asymmetry factor g are different at different depths, and thus the scattering angles of scattered photons from seawater are different at different depths.

After determining the absorption coefficient, the scattering coefficients at different depths and the scattering angle of scattered photons from seawater, this paper will analyze the forward coverage range for blue-green light NLOS transmission to ensure that the receiver is within that range, making blue-green light NLOS transmission possible for communication.

3. Non-Line-of-Sight Transmission Single Scattering Link Model

3.1. Scattering Coverage Analysis

There are two forms of blue-green light NLOS transmission in seawater as follows, named as class a form and class b form, as shown in **Figure 2**.

In this paper, r indicates the separation distance between the laser and the PD, *i.e.*, the communication distance for blue-green light NLOS transmission, θ_t denotes the transmitting deflection angle of the laser, θ_r denotes the receiving deflection angle of the PD, φ_t denotes the beam divergence angle of the laser, and φ_r denotes the receiving field-of-view angle of the PD. In the form of class a, θ_t and θ_r cannot be 90° at the same time (we take $0^\circ < \theta_t < 90^\circ$ and $\theta_r = 90^\circ$), in class b form, $0^\circ < \theta_t < 90^\circ$, $0^\circ < \theta_r < 90^\circ$. The projection of the scattering coverage for a class a form of NLOS transmission is shown in **Figure 3** [26].

In this paper, A denotes the laser, B denotes the PD, r_1 denotes the distance from the laser to the effective scatterer, and r_2 denotes the distance from the effective scatterer to the PD. In **Figure 3(a)**, AO is the central axis of the laser beam and BK is the central axis of the received field of view of the PD. In **Figure 3(b)**, the class a form forward scattering coverage is elliptical arc \widehat{EMDF} , and for backscattering an approximate correction is made using an arc of radius $B'D$

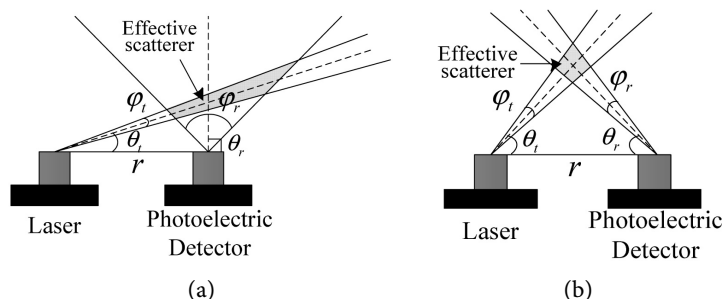


Figure 2. Blue-green light NLOS transmission methods. (a) class a form; (b) class b form.

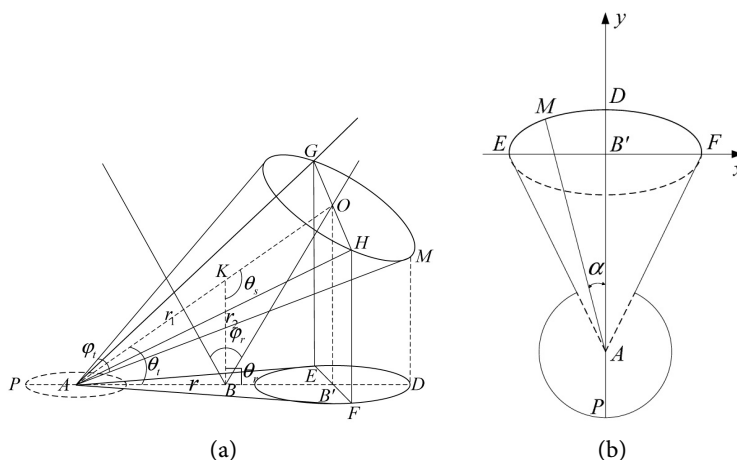


Figure 3. Projection of the scattering coverage of class a form. (a) Coverage projection stereogram; (b) Coverage projection plan.

of the short half-axis of the forward scattering ellipse arc. Take any point M on the elliptical arc \widehat{EMDF} , let the coordinates of the point M be (x_0, y_0) , the angle between AM and y -axis is α , and let the elliptical equation of the ellipse where the elliptical arc \widehat{EMDF} is located be

$$\frac{x^2}{a^2} + \frac{y^2}{b^2} = 1 \tag{23}$$

where the long semi-axis a and short semi-axis b of the ellipse are

$$a = \frac{EF}{2} = B'F = \tan\left(\frac{\varphi_t}{2}\right) \frac{r \cos\left(\frac{\varphi_r}{2}\right)}{\cos\left(\theta_t + \frac{\varphi_r}{2}\right)} \tag{24}$$

$$b = B'D = \frac{r \tan\left(\frac{\varphi_t}{2}\right)}{\cot \theta_t - \tan\left(\frac{\varphi_r}{2}\right)} \tag{25}$$

Let the equation of the line AM be

$$y = kx + c \tag{26}$$

where the slope k of the line and the intercept c on the y -axis are

$$k = -\cot \alpha \tag{27}$$

$$c = -\frac{r \cos \theta_t \cos\left(\frac{\varphi_r}{2}\right)}{\cos\left(\theta_t + \frac{\varphi_r}{2}\right)} \tag{28}$$

From the equation of the ellipse in which the ellipse arc \widehat{EMDF} is located and the equation of the line in which the line AM is located, the coordinates of

the point A are $\left(0, -\frac{r \cos \theta_t \cos\left(\frac{\varphi_r}{2}\right)}{\cos\left(\theta_t + \frac{\varphi_r}{2}\right)}\right)$. The horizontal coordinate x_0 of the

point M is

$$x_0 = -\frac{r \cos \frac{\varphi_r}{2} \cos \theta_t \cot \alpha \cos^2 \frac{\varphi_r}{2} \left(\cot \theta_t - \tan \frac{\varphi_r}{2}\right)^2 + r \cos \frac{\varphi_r}{2} \sqrt{K_2}}{K_1} \tag{29}$$

where

$$K_1 = \cos^3\left(\theta_t + \frac{\varphi_r}{2}\right) + \cos\left(\theta_t + \frac{\varphi_r}{2}\right) \cot^2 \alpha \cos^2 \frac{\varphi_r}{2} \left(\cot \theta_t - \tan \frac{\varphi_r}{2}\right)^2 \tag{30}$$

$$\begin{aligned} K_2 = & -\cos^2 \frac{\varphi_r}{2} \cos^2 \theta_t \left(\cot \theta_t - \tan \frac{\varphi_r}{2}\right)^2 \cos^2\left(\theta_t + \frac{\varphi_r}{2}\right) \\ & + \tan^2 \frac{\varphi_r}{2} \cos^4\left(\theta_t + \frac{\varphi_r}{2}\right) + \tan^2 \frac{\varphi_r}{2} \cos^2 \frac{\varphi_r}{2} \cos^2\left(\theta_t + \frac{\varphi_r}{2}\right) \\ & \times \cot^2 \alpha \left(\cot \theta_t - \tan \frac{\varphi_r}{2}\right)^2 \end{aligned} \tag{31}$$

The vertical coordinate y_0 of the point M is

$$y_0 = -x_0 \cot \alpha - \frac{r \cos \theta_i \cos \frac{\varphi_r}{2}}{\cos \left(\theta_i + \frac{\varphi_r}{2} \right)} \tag{32}$$

where the maximum value of angle α is half of φ . From the equation of the distance between two points, we get

$$|AM| = \sqrt{x_0^2 + \left[y_0 + \frac{r \cos \theta_i \cos \left(\frac{\varphi_r}{2} \right)}{\cos \left(\theta_i + \frac{\varphi_r}{2} \right)} \right]^2} \tag{33}$$

where $|AM|$ is the forward scattering coverage of class a form of NLOS transmission, and the radius AP of the backscattering correction circle is equal to the short semi-axis $B'D$ of the forward scattering ellipse, so the backscattering coverage of class a form is approximately $B'D$. From Equations (33) and (25), it can be seen that $|AM|$ and $B'D$ are independent of the scattering angle as well as the wavelength of light.

The projection of the scattering coverage for the class b form of NLOS transmission is shown in **Figure 4** [26].

In **Figure 4**, φ_1 is the projection of the beam divergence angle of the laser on the horizontal plane, and φ_2 is the angle between BN and BT . As can be seen from **Figure 4**, the scattering coverage of the class b form increases the triangular coverage area on the basis of the class a form, at which time the backscattering is small and negligible.

For the form of class b, the coordinates of point A is $\left(0, -\frac{r \cos \theta_i \cos \left(\frac{\varphi_r}{2} \right)}{\cos \left(\theta_i + \frac{\varphi_r}{2} \right)} \right)$

and the coordinates of point B is $(0, r_2 \cos \theta_i)$. In the class b form, the forward

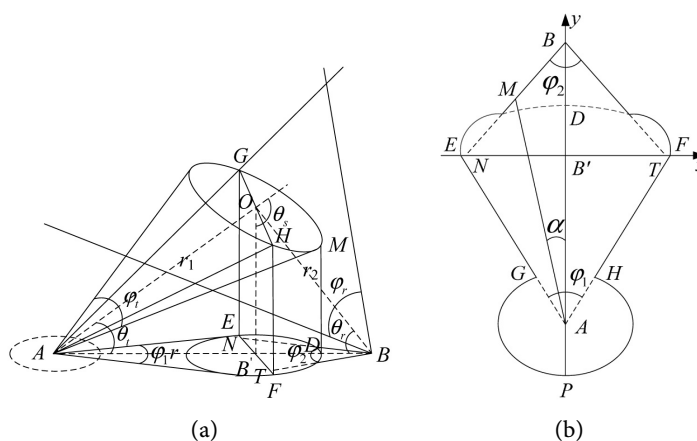


Figure 4. Projection of the scattering coverage of class b form. (a) Coverage projection stereogram; (b) Coverage projection plan.

scattering coverage is the distance from point A to the arc when $\varphi_2 \geq \varphi_1$, however, when $\varphi_2 \leq \varphi_1$, the forward scattering coverage becomes the distance from point A to the straight line BN .

The equation of the straight line BN is

$$x \cot\left(\frac{\varphi_2}{4}\right) - y + \frac{r \sin \theta_t \cos \theta_r}{\sin \theta_s} = 0 \tag{34}$$

The equation for the distance from a point to a line gives

$$\begin{aligned} |AM| &= \frac{|Ax_0 + By_0 + C|}{\sqrt{A^2 + B^2}} \\ &= \left| \sin\left(\frac{\varphi_2}{2}\right) \left| \frac{r \cos \theta_t \cos\left(\frac{\varphi_r}{2}\right)}{\cos\left(\theta_t + \frac{\varphi_r}{2}\right)} + \frac{r \sin \theta_t \cos \theta_r}{\sin \theta_s} \right| \right| \end{aligned} \tag{35}$$

Therefore, for $\varphi_2 \leq \varphi_1$, the forward scattering coverage of the class b form is $|AM|$ in **Figure 4**. From Equation (35), it can be seen that the forward scattering coverage of the class b form is related to the scattering angle θ_s . The following is an analysis of the received optical power and BER of the PD when blue-green light NLOS transmission in class a form and class b form.

3.2. Received Optical Power and BER

According to **Figure 2(a)** we can get the single scattering link model when blue-green light NLOS transmission in class a form, as shown in **Figure 5**.

The volume V_a of the effective scatterer of class a form can be approximated as the volume of the large cone (cone of height h_1) minus the volume of the small cone (cone of height h_2). So, the expression of V_a is [26]

$$V_a = \frac{\pi}{3} r^3 \tan^2\left(\frac{\varphi_r}{2}\right) \left[\tan^3\left(\theta_t + \frac{\varphi_t}{2}\right) - \tan^3\left(\theta_t - \frac{\varphi_t}{2}\right) \right] \tag{36}$$

According to reference [27], we can obtain the received optical power of the PD P_{ra} in class a form as

$$P_{ra} = \frac{P_T b_{sea}(\lambda) P_{HG}(\theta, g) \cos \xi \exp[-c_{sea}(\lambda)(r_1 + r_2)] A_r V_a}{\Omega_t r_1^2 r_2^2} \tag{37}$$

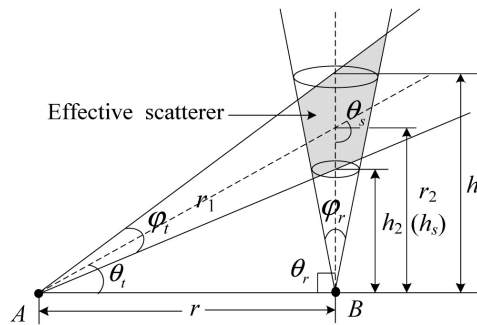


Figure 5. Class a form of NLOS transmission single scattering link model.

where P_T is the emitted optical power of the laser, A_r is the area of the receiving antenna, Ω_r is the stereo angle of the emitted beam of the laser, and ξ is the angle between the transmitting light cone and the receiving light cone. We set $\xi = 0^\circ$, *i.e.*, the emitting light cone is coplanar with the receiving light cone. The expressions for r_1 and r_2 are easily obtained from the geometric relations of the triangle. The expression of Ω_r is [27]

$$\Omega_r = 2\pi \left(1 - \cos \frac{\varphi_l}{2} \right) \tag{38}$$

From Equation (37), the received optical power of the PD is related to $P_{HG}(\theta, g)$, $b_{sea}(\lambda)$ and $c_{sea}(\lambda)$, while $P_{HG}(\theta, g)$, $b_{sea}(\lambda)$ and $c_{sea}(\lambda)$ are all related to the depth of seawater. The depth of the effective scatterer in seawater h_{as} is obtained as the depth of the laser in seawater h minus the distance h_s ($h_s = r_2$ in the class a form) of the effective scatterer from the LOS link between the laser and the PD.

$$h_{as} = h - h_s = h - r_2 = h - \frac{r \sin \theta_l}{\sin(\pi - \theta_l - \theta_r)} \tag{39}$$

From **Figure 2(b)**, the single scattering link model of NLOS transmission in class b form is shown in **Figure 6**.

The volumes of the effective scatterers $V_{A_1B_1C_1D_1}$ and $V_{E_1F_1G_1H_1}$ are

$$V_{A_1B_1C_1D_1} = \frac{\pi}{3} \tan^2 \left(\frac{\varphi_l}{2} \right) \left\{ \left[r_1 + \frac{r_2 \tan \frac{\varphi_r}{2}}{\left(\tan \theta_s + \tan \frac{\varphi_r}{2} \right) \cos \theta_s} \right]^3 - \left[r_1 - \frac{r_2 \sin \frac{\varphi_r}{2}}{\sin \left(\theta_s - \frac{\varphi_r}{2} \right)} \right]^3 \right\} \tag{40}$$

$$V_{E_1F_1G_1H_1} = \frac{\pi}{3} \tan^2 \left(\frac{\varphi_r}{2} \right) \left\{ \left[r_2 + \frac{r_1 \tan \frac{\varphi_l}{2}}{\left(\tan \theta_s + \tan \frac{\varphi_l}{2} \right) \cos \theta_s} \right]^3 - \left[r_2 - \frac{r_1 \sin \frac{\varphi_l}{2}}{\sin \left(\theta_s - \frac{\varphi_l}{2} \right)} \right]^3 \right\} \tag{41}$$

The volume V_b of the effective scatterer in the class b form is the smallest of $V_{A_1B_1C_1D_1}$ and $V_{E_1F_1G_1H_1}$, *i.e.*, $V_b = \min(V_{A_1B_1C_1D_1}, V_{E_1F_1G_1H_1})$.

By replacing V_a with V_b in Equation (37), the received optical power of the PD P_{rb} can be obtained when the blue-green light NLOS transmission in class b form. The depth of the effective scatterer in seawater in class b form h_{bs} is h minus h_s .

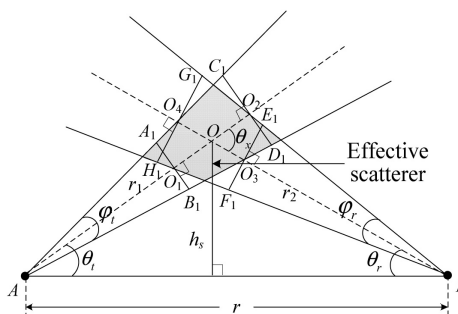


Figure 6. Class b form NLOS transmission single scattering link model.

$$h_{bs} = h - h_s = h - \frac{r \sin \theta_r \sin \theta_t}{\sin(\pi - \theta_t - \theta_r)} \quad (42)$$

Assuming that a PIN PD is used at the receiver, the noise current i_n^2 of the PIN PD mainly consists of thermal noise i_t^2 , scattering noise i_{sh}^2 and dark current noise i_{dark}^2 [28].

$$i_n^2 = i_t^2 + i_{sh}^2 + i_{dark}^2 = \frac{4k_B T_{PIN} B}{R} + 2eI_s B + 2eI_D B \quad (43)$$

where B is the bandwidth of the PD, assuming that the bandwidth of the PD is two times the information transmission rate, that is, $B = 2R_b$, R is the load resistance, according to engineering experience $R = 50 \Omega$, T_{PIN} is the absolute temperature of the PIN PD work, e is the electronic charge, I_s is the signal light reaches the PD generated by the light current and I_D is the dark current.

$$I_s = \frac{e\eta}{h\nu} P_s \quad (44)$$

where η is the quantum efficiency, h is Planck's constant, ν is the frequency of light and P_s is the received optical power of the PD. In the form of class a, $P_s = P_{rb}$ and in the form of class b, $P_s = P_{rb}$. The output SNR of the PD is

$$SNR = \frac{e^2 \eta^2 P_s^2}{h^2 \nu^2 i_n^2} \quad (45)$$

The blue-green light is modulated by the external modulator as on-off keying (OOK) signal, and the BER at the receiver of the system is

$$P_e = \frac{1}{2} \operatorname{erfc} \left(\sqrt{\frac{SNR}{4}} \right) \quad (46)$$

After obtaining the forward scattering coverage of blue-green light under different forms of NLOS transmission, we will set the simulation parameters of transmitting deflection angle, beam divergence angle, receiving deflection angle and receiving field of view angle to analyze the characteristics of blue-green light during NLOS transmission in the forms of class a and class b in seawater of different depths.

4. Simulation Analysis

Simulation analysis blue-green light NLOS transmission in class a form and class b form in seawater at different depths, let $P_T = 1 \text{ W}$, $I_D = 10 \text{ nA}$, $\eta = 0.6$, $A_r = 0.04\pi \text{ m}^2$, $r = 12 \text{ m}$.

4.1. Class a Form

The simulation results of the received optical power and BER of the PD for 450 nm blue light and 520 nm green light NLOS transmission in class a form are shown in **Figure 8**. In the simulation, $\varphi_t = 30^\circ$, $\varphi_r = 110^\circ$ and $\alpha = 10^\circ$. Before the simulation, it is verified that the position of the PD is located within the forward scattering range of the laser according to Equation (33).

Figure 7 shows the forward scattering coverage of the laser increases with the increase of the emission deflection angle. The location of the PD under the given simulation conditions is always within the forward scattering coverage of the laser, *i.e.*, the PD is able to receive the optical signal.

Figure 8(a) and **Figure 8(b)** show the received optical power of the PD is in the overall decreasing trend with the increase of the emission deflection angle, and the decreasing trend is similar to the exponential form, so reducing the emission deflection angle of the laser can effectively increase the received optical power of the system. The received optical power of blue-green light increases with the increase of seawater depth for the same emission deflection angle. This is because the deeper the seawater, the smaller the scattering coefficient of seawater, the less scattering effect on blue-green light. With the same emission deflection angle, the received optical power of 520 nm green light is greater than that of 450 nm blue light. **Figure 8(c)** shows the BER at the receiver for different information transmission rates when the transmitting deflection angle of the laser is 5° . The BER at the receiver side decreases with the increase of seawater depth for the same information transmission rate. With the BER of less than 10^{-6} , blue-green light can achieve an information transmission rate of more than 100 Mbps with NLOS transmission in class a form at the depth of 690 m.

4.2. Class b Form

The simulation results of the received optical power and BER of the PD for blue-green light NLOS transmission in the form of class b are shown in **Figure 10**, taking $\theta_t = 37^\circ$, $\varphi_t = 30^\circ$ and $\varphi_r = 110^\circ$. The location of the PD is verified to be within the forward scattering range of the laser according to Equation (35) before the simulation.

Figure 9 shows the forward scattering coverage of the laser is in an overall increasing trend with the increase of the receiving deflection angle. The location of the PD under the given simulation conditions is always within the forward scattering coverage of the laser.

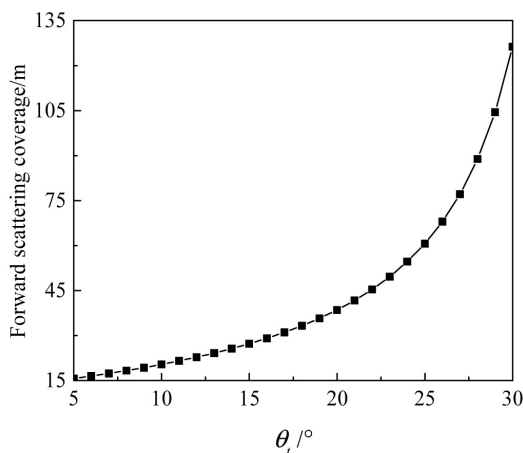
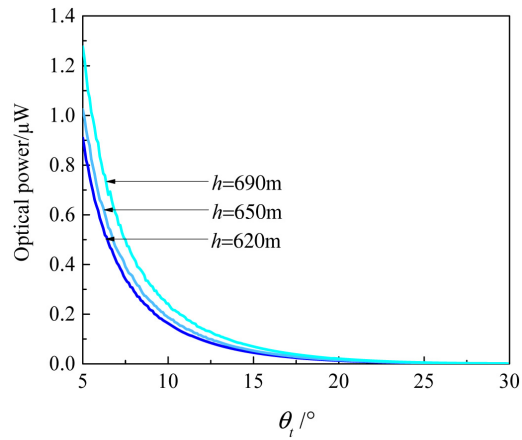
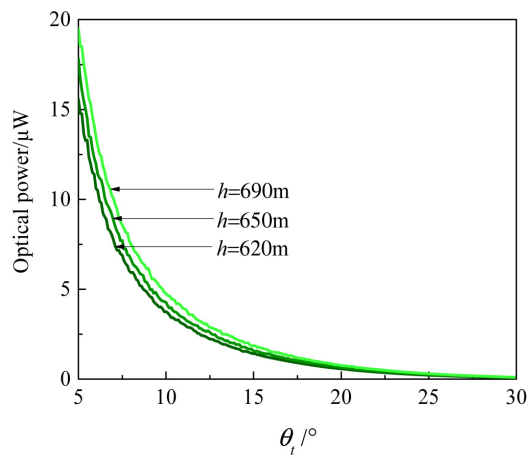


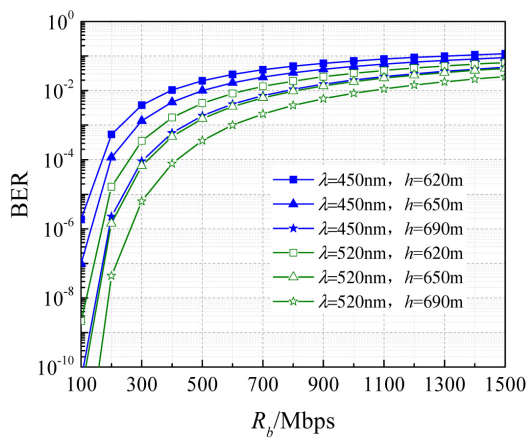
Figure 7. Forward scattering coverage in the form of class a.



(a)



(b)



(c)

Figure 8. Received optical power and BER of NLOS transmission in the form of class a. (a) $\lambda = 450$ nm; (b) $\lambda = 520$ nm; (c) BER.

Figure 10(a) and **Figure 10(b)** show the received optical power of the PD with the increase of the received deflection angle is in the overall decreasing trend, the same decreasing trend is similar to the exponential form, so reduce

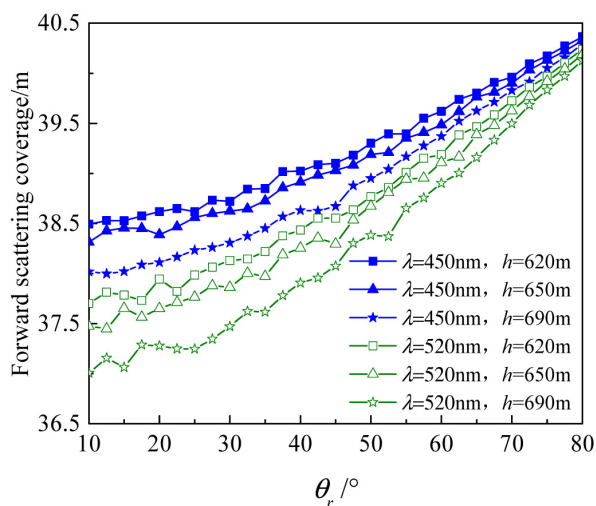
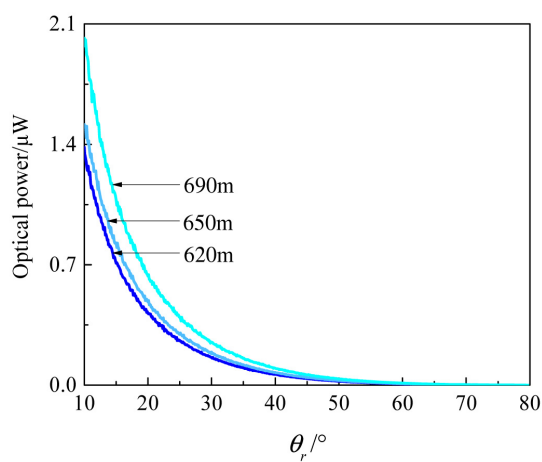
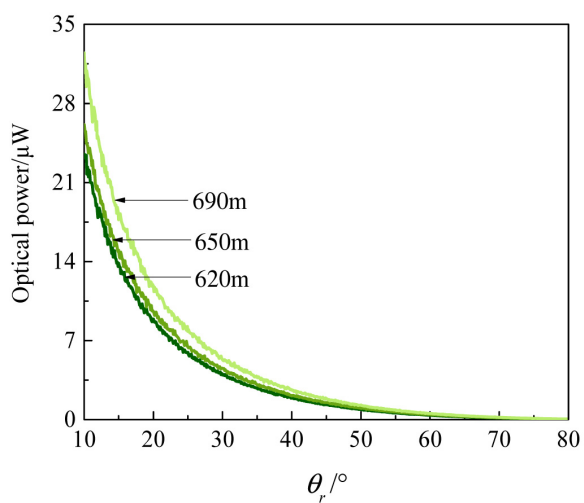


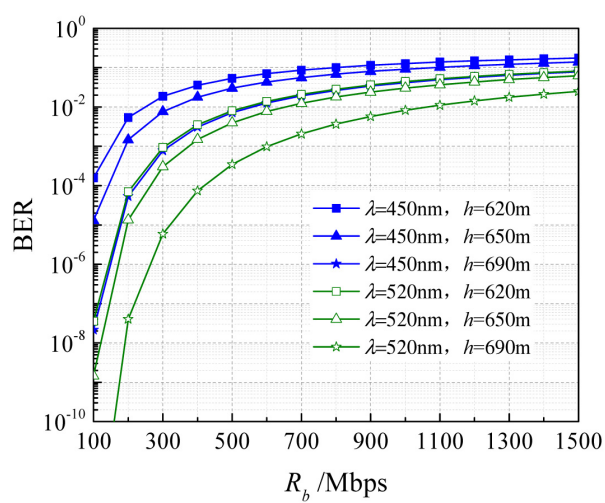
Figure 9. Forward scattering coverage in the form of class b.



(a)



(b)



(c)

Figure 10. Received optical power and BER of NLOS transmission in the form of class b. (a) $\lambda = 450$ nm; (b) $\lambda = 520$ nm; (c) BER.

the received deflection angle of the PD can effectively increase the received optical power of the system. The same as class a form, when blue-green light NLOS transmission in class b form, the received optical power of blue-green light increases with the depth of seawater under the same receiving deflection angle, and the received optical power of 520 nm green light is greater than that of 450 nm blue light. **Figure 10(c)** shows the BER at the receiver end for different information transmission rates with a receive deflection angle of 15° for blue light and 50° for green light. Also with BER less than 10^{-6} , blue-green light can achieve an information transmission rate of more than 100 Mbps with NLOS transmission in class b form at the depth of 690 m.

5. Conclusions

This paper calculates the absorption and scattering coefficients of seawater are calculated, the scattering coverage of blue-green light in seawater in class a form and class b form for NLOS transmission, as well as the received optical power and BER of the PD. The analysis results show that when the blue-green light NLOS transmission in class a form and class b form, increasing the transmit deflection angle of the laser and the receive deflection angle of the PD can increase the forward scattering coverage of the laser, but will reduce the received optical power of the PD. Therefore, when the actual UWOC is carried out, appropriate trade-offs should be made between the forward scattering coverage of the laser and the received optical power of the PD, in order to realize that the receiver is within the forward scattering coverage of the laser, but also to make the receiver receive as much optical power as possible. When NLOS UWOC, the choice of green light can effectively increase the received optical power of the PD and reduce the BER. In addition, when NLOS UWOC is in the same way in seawater at different depths, the emitted optical power of the laser should be adjusted to achieve NLOS communication with the same information transmission rate and the same distance.

In this paper, only the case when the transmitting and receiving optical cones are coplanar, *i.e.*, $\xi = 0^\circ$, is considered, so that the received optical power and BER at the receiver can be considered for different depths of NLOS transmission when non-coplanar in the future work.

Acknowledgements

This work was supported by Key Industry Innovation Chain Project of Shaanxi Province of China (2017ZDCXL-GY-06-01), Xi'an Science and Technology Innovation Guidance Project of China (201805030YD8CG14(12)).

Conflicts of Interest

The authors declare no conflicts of interest regarding the publication of this paper.

References

- [1] Duntley, S.Q. (1963) Light in the Sea. *Journal of the Optical Society of America*, **53**, 214-233. <https://doi.org/10.1364/JOSA.53.000214>
- [2] Hale, G.M. and Querry, M.R. (1973) Optical Constants of Water in the 200-nm to 200- μ m Wavelength Region. *Applied Optics*, **12**, 555-563. <https://doi.org/10.1364/AO.12.000555>
- [3] Pope, R.M. and Fry, E.S. (1997) Absorption Spectrum (380-700 nm) of Pure Water. II. Integrating Cavity Measurements. *Applied Optics*, **36**, 8710-8723. <https://doi.org/10.1364/AO.36.008710>
- [4] Cochenour, B.M., Mullen, L.J. and Laux, A.E. (2008) Characterization of the Beam-Spread Function for Underwater Wireless Optical Communications Links. *IEEE Journal of Oceanic Engineering*, **33**, 513-521. <https://doi.org/10.1109/JOE.2008.2005341>
- [5] Zeng, Z.Q., Fu, S., Zhang, H.H., Dong, Y.H. and Cheng, J.L. (2017) A Survey of Underwater Optical Wireless Communications, *IEEE Communications Surveys & Tutorials*, **19**, 204-238. <https://doi.org/10.1109/COMST.2016.2618841>
- [6] Kaushal, H. and Kaddoum, G. (2016) Underwater Optical Wireless Communication. *IEEE Access*, **4**, 1518-1547. <https://doi.org/10.1109/ACCESS.2016.2552538>
- [7] Zhu, S.J., Chen, X.W., Liu, X.Y., Zhang, G.Q. and Tian, P.F. (2020) Recent Progress in and Perspectives of Underwater Wireless Optical Communication. *Progress in Quantum Electronics*, **73**, Article ID: 100274. <https://doi.org/10.1016/j.pquantelec.2020.100274>
- [8] Hu, L.B., Zhang, X.D. and Perry, M.J. (2020) Light Scattering by Pure Seawater at Subzero Temperatures. *Deep-Sea Research Part I*, **162**, Article ID: 103306. <https://doi.org/10.1016/j.dsr.2020.103306>
- [9] Zhang, X.D., Hu, L.B. and He, M.X. (2009) Scattering by Pure Seawater: Effect of Salinity. *Optics Express*, **17**, 5698-5710. <https://doi.org/10.1364/OE.17.005698>
- [10] Hu, L.B., Zhang, X.D. and Perry, M.J. (2019) Light Scattering by Pure Seawater: Effect of Pressure. *Deep-Sea Research Part I*, **146**, 103-109. <https://doi.org/10.1016/j.dsr.2019.03.009>
- [11] Haltrin, V.I. (1999) Chlorophyll-Based Model of Seawater Optical Properties. *Applied Optics*, **38**, 6826-6832. <https://doi.org/10.1364/AO.38.006826>
- [12] Arnon, S. and Kedar, D. (2009) Non-Line-of-Sight Underwater Optical Wireless Communication Network. *Journal of the Optical Society of America A*, **26**, 530-539. <https://doi.org/10.1364/JOSAA.26.000530>
- [13] Jagadeesh, V.K., Choudhary, A., Bui, F.M. and Muthuchidambaranathan, P. (2014) Characterization of Channel Impulse Responses for NLOS Underwater Wireless Optical Communications. 2014 *Fourth International Conference on Advances in Computing and Communications*, Cochin, 27-29 August 2014, 77-79. <https://doi.org/10.1109/ICACC.2014.24>
- [14] Liu, W.H., Zou, D.F., Xu, Z.Y. and Yu, J.C. (2015) Non-Line-of-Sight Scattering Channel Modeling for Underwater Optical Wireless Communication. 2015 *IEEE International Conference on Cyber Technology in Automation, Control, and Intelligent Systems*, Shenyang, 8-12 June 2015, 1265-1268. <https://doi.org/10.1109/CYBER.2015.7288125>
- [15] Sait, M., Sun, X.B., Alkhazragi, O., Alfaraj, N., Kong, M.W., Ng, T.K. and Ooi, B.S. (2019) The Effect of Turbulence on NLOS Underwater Wireless Optical Communication Channels. *Chinese Optics Letters*, **17**, Article ID: 100013.

- <https://doi.org/10.3788/COL201917.100013>
- [16] Priyalakshmi, B. and Mahalakshmi, K. (2020) Channel Estimation and Error Correction for UWOC System with Vertical Non-Line-of-Sight Channel. *Wireless Networks*, **26**, 4985-4997. <https://doi.org/10.1007/s11276-020-02376-2>
- [17] Sait, M., Guo, Y.J., Alkhazragi, O., Kong, M.W., Ng, T.K. and Ooi, B.S. (2021) The Impact of Vertical Salinity Gradient on Non-Line-of-Sight Underwater Optical Wireless Communication. *IEEE Photonics Journal*, **13**, Article ID: 7300609. <https://doi.org/10.1109/JPHOT.2021.3121169>
- [18] Prieur, L. and Sathyendranath, S. (1981) An Optical Classification of Coastal and Oceanic Waters Based on the Specific Spectral Absorption Curves of Phytoplankton Pigments, Dissolved Organic Matter, and Other Particulate Materials. *Limnology and Oceanography*, **26**, 671-689. <https://doi.org/10.4319/lo.1981.26.4.0671>
- [19] Feistel, R. (2003) A New Extended Gibbs Thermodynamic Potential of Seawater. *Progress in Oceanography*, **58**, 43-114. [https://doi.org/10.1016/S0079-6611\(03\)00088-0](https://doi.org/10.1016/S0079-6611(03)00088-0)
- [20] Feistel, R. (2008) A Gibbs Function for Seawater Thermodynamics for -6 to 80 °C and Salinity Up to 120g kg^{-1} . *Deep Sea Research Part I: Oceanographic Research Papers*, **55**, 1639-1671. <https://doi.org/10.1016/j.dsr.2008.07.004>
- [21] Ji, T.Y., Jiang, G.R., Shi, J., Zhou, Z.G. and Deng, B. (2015) Conversion Methods of Depth and Pressure in the Ocean. *Marine Forecasts*, **32**, 45-50.
- [22] Poulin, C., Zhang, X.D., Yang, P. and Huot, Y. (2018) Diel Variations of the Attenuation, Backscattering and Absorption Coefficients of Four Phytoplankton Species and Comparison with Spherical, Coated Spherical and Hexahedral Particle Optical Models. *Journal of Quantitative Spectroscopy & Radiative Transfer*, **217**, 288-304. <https://doi.org/10.1016/j.jqsrt.2018.05.035>
- [23] Shifrin, K.S. (1988) Physical Optics of Ocean Water. American Institute of Physics, New York.
- [24] Gabriel, C., Khalighi, M.A., Bourennane, S. Leon, P. and Rigaud, V. (2013) Monte-Carlo-Based Channel Characterization for Underwater Optical Communication Systems. *IEEE/OSA Journal of Optical Communications & Networking*, **5**, 1-12. <https://doi.org/10.1364/JOCN.5.000001>
- [25] Mobley, C.D., Sundman, L.K. and Boss, E. (2002) Phase Function Effects on Oceanic Light Fields. *Applied Optics*, **41**, 1035-1050. <https://doi.org/10.1364/AO.41.001035>
- [26] Ke, X.Z. (2011) Ultraviolet Self-Organizing Network Theory. Science Press, Beijing.
- [27] Wu, T.F., Ma, J.S., Su, P., Yuan, R.Z. and Cheng, J.L. (2019) Modeling of Short-Range Ultraviolet Communication Channel Based on Spherical Coordinate System. *IEEE Communications Letters*, **23**, 242-245. <https://doi.org/10.1109/LCOMM.2018.2890518>
- [28] Xu, F., Khalighi, M.A. and Bourennane, S. (2011) Impact of Different Noise Sources on the Performance of PIN- and APD-Based FSO Receivers. *11th International Conference on Telecommunications*, Graz, 15-17 June 2011, 211-218.